International Journal of Heat and Mass Transfer 135 (2019) 974–984

Contents lists available at ScienceDirect

International Journal of Heat and Mass Transfer

journal homepage: www.elsevier.com/locate/ijhmt

Three mathematical representations and an improved ADI method for hyperbolic heat conduction

Ben-Dian Nie, Bing-Yang Cao *

Key Laboratory for Thermal Science and Power Engineering of Ministry of Education, Department of Engineering Mechanics, Tsinghua University, Beijing 100084, China

ARTICLE INFO

Article history:
Received 24 August 2018
Received in revised form 8 December 2018
Accepted 10 February 2019

Keywords:
Hyperbolic heat conduction
Alternative direction implicit (ADI)
Characteristics analyses
Vector characteristics
Thermal wave

ABSTRACT

Hyperbolic heat conduction models have been proposed to characterize the breakdown of Fourier's law, i.e. thermal waves. In this paper, three mathematical representations for hyperbolic heat conduction, namely temperature representation, hybrid representation and heat flux representation, and their corresponding characteristics are first analyzed. The hybrid representation is demonstrated to be preferable for numerical calculations and contains sufficient heat transport information. Specifically designed for solving transient heat conduction problems in the hybrid representation, an improved alternative direction implicit (ADI) method based on staggered grids is then developed. This algorithm focuses on the entire hyperbolic equation set instead of one single hyperbolic equation, and it adopts chasing method rather than iteration, which enables to significantly save computing time and storage space. Characteristics analyses on the definite conditions show that for each side only one boundary condition is necessary for Cattaneo-Vernotte (CV) type hyperbolic heat conduction. The advantages of the hybrid representation are also demonstrated by numerical simulations. Besides, the initial heat flux, which implies the initial phonon momentum in dielectrics, has an important influence on the propagation patterns of thermal waves, changing the way of energy conveying. The mechanism of phonon momentum conservation leads to the vector characteristics of thermal waves, and causes the direction preference in hyperbolic heat conduction.

1. Introduction

Conventional Fourier's heat conduction law leads to the paradox of infinite thermal perturbation speed due to the nature of diffusion equation [1]. Hyperbolic heat conduction equations (HHCE) were then proposed, implying that the thermal energy propagates in a media in a wavelike behavior and introducing the concept of thermal wave [2–4]. Thermal wave is related to the experimental observations of second sound [5–9] and time delay [10]. With the development of ultrafast laser heating and nanoscale material fabrication, many heat conduction phenomena cannot be described by Fourier's law, calling for a new understanding of hyperbolic heat transport mechanism. In the past few decades, hyperbolic heat conduction has been widely investigated and applied in the field of nano-electromechanical systems [3,4], biological medicine [11,12], material flaw analysis [13], functional graded materials [14,15] and so on.

Many hyperbolic models have been proposed from different views and scales. Cattaneo and Vernotte [16,17] developed the first mathematical hyperbolic heat conduction equation, namely Cattaneo-Vernotte (CV) equation. Guyer and Krumhansl [18,19] solved the linearized phonon Boltzmann equation and derived the hydrodynamics model. Green and Laws [20] postulated a new entropy inequality and gave a damped wave equation by linearized simplification. Tzou [10,21] explored the heat conduction phenomena in metals and developed the single phase lag model into dual phase lag model, while in the further investigations it is demonstrated that the dual phase lag model might lead to non-well posed problems and cause unphysical defects [22–25]. Guo *et al.* [26–28] established the thermomass model based on the equality between thermal energy and mass, and derived the motion equations of thermomass. Multiple terms are included in these models causing the non-Fourier effects such as inertial effect, nonlocal effect and nonlinearity [29]. Multiple effects and their coupled reaction make the heat conduction more complex. Inertial effect is especially significant, which leads the parabolic equation into a hyperbolic one. In this paper, the inertial effect is focused on while other effects are ignored, for a better understanding of hyperbolic heat conduction. CV equation is the best choice,

* Corresponding author.
E-mail address: caoby@tsinghua.edu.cn (B.-Y. Cao).

https://doi.org/10.1016/j.ijheatmasstransfer.2019.02.026
0017-9310/

Nomenclature

Letters

A	coefficient matrix for x_1
B	coefficient matrix for x_2
C	coefficient matrix for x_3
D	nonhomogeneous term
G	coefficient matrix
I	unit matrix
M	domain symbol
U	variable vector upper triangular matrix
q	heat flux
m	unit vector
F	nonhomogeneous vector term
L	lower triangular matrix
l	position vector
w	intermediate variable vector
z	node algebraic vector
A	amplitude of heat flux
C_v	volume specific heat
f	arbitrary known function
g	arbitrary known function
m	arbitrary known function
k	thermal conductivity
L	length scale of regime
E	inner energy
n	number of dimensions component of unit vector
T	temperature
t	time
x	coordinates of the domain
y	coordinates of the domain

Greek symbols

τ	relaxation time
λ	characteristic face
α	thermal diffusivity
ρ	mass density
θ	coefficient vector

Superscripts

T	transposition

Subscripts

1, 2, 3	index
0	initial state
i	component of vector
j	component of vector

$$\mathbf{q} + \tau \frac{\partial \mathbf{q}}{\partial t} = -k\nabla T, \tag{1}$$

where $\mathbf{q}$ and T represent the heat flux and local temperature, respectively. τ is the relaxation time and k is the thermal conductivity. CV equation promotes the heat flux field to a more independent level, making the whole equation set own vector characteristics. The whole hyperbolic equation set consists of the energy conservation equation,

$$\rho C_v \frac{\partial T}{\partial t} + \nabla \cdot \mathbf{q} = 0, \tag{2}$$

and CV equation (Eq. (1)). The hyperbolic characteristics of the equation set lead to strongly directional preference and more propagation phenomena different from conventional heat conduction [30]. There is also a big difference in the analytical methods between hyperbolic equations and parabolic equations, which will be discussed in detail in the following sections.

Numerical simulations has been studied for thermal waves in the past few decades [31–37], most of which focus on one-dimensional problems. Zhang *et al.* [38,39] studied the damping and dispersion of thermal waves and made it clear how thermal waves propagate. However, the vector characteristics are ignored because its influences take effect only in multidimensional heat conduction. Yang [40] proposed a high-resolution numerical method to solve two-dimensional linear HHCE with constant thermal properties. Chen and Lin [41] then studied the problems with temperature-dependent thermal properties via a hybrid application of the Laplace transform and control-volume formulation. Shen and Han [42] dealt with nonlinear boundary conditions and used characteristic relationship to find the unknown boundary condition value (either heat flux or temperature) and an explicit Total Variation Diminishing (TVD) scheme was adopted. Wu and Li [43] introduced the discontinuous Galerkin finite element method to solve two-dimensional HHCE problems. Moosaie *et al.* [44] gave an analytical solution for a rectangular regime with arbitrary initial conditions and periodic boundary conditions based on superposition solution, which as mentioned could be used as a benchmark. Ma *et al.* [45] pushed forward to give the analytical solution for a square plate subjected to a moving laser pulse. Yang [46] deduced an inverse solution from a finite difference method, the concept of future time and a modified Newton-Raphson method to estimate boundary conditions of the two-dimensional hyperbolic heat conduction problems. Recently, Rieth *et al.* [47] developed an implicit form of finite difference method to solve the Guyer-Krumhansl equation and demonstrated that the Crank-Nicolson-type implicit scheme is the most accurate. Most of them treated the problem as the extension of Fourier's heat conduction, ignoring the fascinating characteristics brought by the hyperbolic effect.

Alternative direction implicit (ADI) method was first proposed to solve parabolic heat conduction problems [48], which was extended to hyperbolic systems shortly afterwards [49]. Douglas *et al.* [50] gave the general formulation of ADI, including both parabolic and hyperbolic problems and enriching the theories. Then, this method has been developed into several unconditionally stable schemes [51,52], which are second-order accurate both in time and in space. As for higher accuracy scheme, compact scheme was combined with ADI method [53–55], some of which are fourth-order accurate both in time and space. Besides, ADI method was also applied to nonlinear hyperbolic systems and the second type boundary conditions (Neumann boundary condition) [56]. However, these updates mainly focus on the second order wave equations. In this paper, it is demonstrated that in hyperbolic heat conduction systems, pure wave equation, even with energy dissipation, is not sufficient and might miss some information, requiring an improved ADI scheme specifically designed for hyperbolic heat conduction.

It is found from all above that hyperbolic heat conduction is quite different from conventional parabolic heat conduction and wave propagation. In order to improve the recognition of the hyperbolic heat conduction systems from both physical and mathematical views, two points are explored below. The analyses of the vector characteristics for hyperbolic heat conduction are expressed

in Section 2 and an improved hybrid ADI method based on staggered grids is developed in Section 3. In Section 4, three numerical examples calculated by the improved ADI method are shown to depict the propagation pattern of thermal waves and highlight the vector nature of heat conduction.

2. Representations and model analyses

2.1. Three mathematical representations

Before talking about the difference between hyperbolic heat conduction and parabolic heat conduction and elastic wave propagation, three different kinds of representations for hyperbolic systems are discussed, namely the temperature representation, the hybrid representation and the heat flux representation. These representations are sorted by the state variables adopted in the equation set.

The temperature representation substitutes the heat flux field with the temperature field and derives a second order telegraph equation, constructed by the energy conservation Eq. (2) and CV Eq. (1),

$$\frac{\partial^2 T}{\partial t^2}+\frac{1}{\tau}\frac{\partial T}{\partial t}=\frac{\alpha}{\tau}\Delta T, \tag{3}$$

where α is the thermal diffusivity,

$$\alpha=\frac{k}{\rho C_v}. \tag{4}$$

Temperature representation is the most common way in solving hyperbolic heat conduction problems, which has obvious advantages. In n-dimensional regimes (n = 1, 2, 3), the hyperbolic equation set consisting of $n+1$ equations is transformed into one single equation with the state variable T. It is convenient for both theoretical solutions and numerical simulations. However, this kind of representation is not so perfect because some information might be missing, which will be discussed in detail in Section 2.2.

In order to solve the equations in the temperature representation, boundary conditions and initial conditions are necessary. In Eq. (3), the highest derivative of temperature field in time is second order, so it calls for two initial conditions. As for each boundary, one boundary condition is required. The initial conditions are supposed to have the form as

$$T(\mathbf{x},t=0)=f_1(\mathbf{x}), \tag{5.1}$$

$$\frac{\partial T}{\partial t}(\mathbf{x},t=0)=g_1(\mathbf{x}), \tag{5.2}$$

where $f_1(x)$ and $g_1(x)$ are two continuous smooth functions, denoting the initial state of temperature field and the temporal derivative, respectively. In this paper, two kinds of boundary conditions are analyzed, namely the adiabatic boundary and isothermal boundary. The adiabatic boundary at the position $\mathbf{x}=\mathbf{l}$ is set to be

$$\frac{\partial T}{\partial x}(\mathbf{x}=\mathbf{l},t)=0. \tag{6}$$

And the isothermal boundary condition at the position $\mathbf{x}=\mathbf{l}$ is set to be

$$T(\mathbf{x}=\mathbf{l},t)=T_0. \tag{7}$$

As for the hybrid representation, it directly uses the heat flux constitutive equation (Eq. (1)) and energy conservation equation (Eq. (2)) to construct the equation set. The representation adopts both temperature and heat flux fields as the state variables, focusing on solving the equation set instead of one single equation. It means that in n-dimensional heat conduction problems, there are $n+1$ state variables influencing each other with their time evolution equations. Of course, Eq. (1) could be changed into any other first-order equation to replace CV equation, making it easy to extend to other thermal wave models easily. Another advantage is that it is convenient for numerical calculations because the time evolution is first order. Compared with the temperature representation, more variables are considered in the hybrid representation, making it more complex and more difficult to directly derive a theoretical solution. The initial conditions require the state of heat flux field and temperature field at the same time to make sure that the problem is well-posed,

$$T(\mathbf{x},t=0)=f_2(\mathbf{x}), \tag{8.1}$$

$$\mathbf{q}(\mathbf{x},t=0)=g_2(\mathbf{x}). \tag{8.2}$$

The adiabatic boundary condition means that there is no heat flux at the boundary, namely

$$\mathbf{q}(\mathbf{x}=\mathbf{l},t)=0. \tag{9}$$

The temperature field is explicit in the representation, so the isothermal boundary can be expressed as

$$T(\mathbf{x}=\mathbf{l},t)=T_0. \tag{10}$$

The heat flux field could also be used as the only state variables, which is called the heat flux representation in this paper. If the temperature field is substituted with the heat flux field in Eqs. (1) and (2), the time evolution equation of heat flux could be expressed as

$$\frac{\partial^2 \mathbf{q}}{\partial t^2}+\frac{1}{\tau}\frac{\partial \mathbf{q}}{\partial t}=\frac{\alpha}{\tau}\nabla(\nabla\cdot\mathbf{q}). \tag{11}$$

Due to the vector nature of heat flux, Eq. (11) includes n equations in n-dimensional heat conduction problems (n = 1, 2, 3). The individual equations in Eq. (11) are

$$\frac{\partial^2 q_i}{\partial t^2}+\frac{1}{\tau}\frac{\partial q_i}{\partial t}=\frac{\alpha}{\tau}\frac{\partial^2 q_j}{\partial x_i \partial x_j}, \tag{12}$$

where q_i represents the component of the heat flux vector and Einstein's summation convention is used to simplify the expression. Actually, rather few researches adopt this kind of representation because it could only give the time evolution of heat flux, compared with which the time evolution of temperature is more familiar and easier to accept. In order to get the temperature distribution profile, it requires the initial temperature distribution as one more initial condition. Therefore, three initial conditions are necessary in total, where two heat flux initial conditions

$$\mathbf{q}(\mathbf{x},t=0)=f_3(\mathbf{x}), \tag{13.1}$$

$$\frac{\partial \mathbf{q}}{\partial t}(\mathbf{x},t=0)=g_3(\mathbf{x}). \tag{13.2}$$

and one temperature initial condition

$$T(\mathbf{x},t=0)=m_3(\mathbf{x}), \tag{13.3}$$

are supposed to be included. These three functions are supposed to be smooth enough. The temperature distribution profile is derived from the energy conservation equation (Eq. (2)) by integrating it with respect to time. The adiabatic boundary condition is expressed as

$$\mathbf{q}(\mathbf{x}=\mathbf{l},t)=0. \tag{14}$$

The isothermal boundary condition requires that the temperature field at the boundary keeps constant while time goes on, so it is expressed as

$$\frac{\partial \mathbf{q}}{\partial \mathbf{x}}(\mathbf{x}=\mathbf{l},t)=0. \tag{15}$$

2.2. Comparisons between the three representations

The temperature representation is the most common one to describe a heat conduction system. The temperature field, analogous with the effect of displacement field in wave equations, varies according to a telegraph equation. Nevertheless, there is an obvious difference between the hyperbolic heat conduction equation and the wave equation. The intermediate variable force field is defined totally by displacement u. That is to say, in the wave equation, if the displacement u is known, the vector force field can be derived from the constitutive equation. However, there are two independent variables in the constitutive equation of hyperbolic heat conduction, namely the heat flux field and the temporal derivative of heat flux field. If the temperature field T is known, the heat flux field which has similar status with the force field in wave equation, cannot be derived. The only thing we make sure is that the sum of heat flux and its derivative equals a known variable,

$$q_i + \tau \frac{\partial q_i}{\partial t} = f(T). \tag{16}$$

Another example is that the adiabatic boundary is not properly assembled in the temperature representation. As shown in Eq. (16), only the following equation is satisfied,

$$q_i + \tau \frac{\partial q_i}{\partial t} = 0. \tag{17}$$

If the derivative of heat flux with respect to time is nonzero, the heat flux at the boundary is also nonzero, which contradicts with the definition of adiabatic boundary. Besides, in temperature representation, the direction information of the initial heat flux is missing. When the derivative of temperature field with respect to time is used as the initial condition, the divergence of heat flux is known, but the initial heat flux distribution is still unknown. In the simulation example 2 in Section 4, it can be seen that the two different problems might have the same expressions for initial conditions using temperature representation and it fails to reveal the differences.

The heat flux representation requires more calculations in order to get the temperature distribution from the energy conservation equation and it includes n second order time evolution equations in total. But its advantages are that all the information is retained so that the vector characteristics are explicitly displayed and as shown in reference [57], heat flux boundary is easy to define. The distribution of heat flux shows the speed of thermal wave propagation, denoting the ability of energy conveying.

The hybrid representation consists of $(n+1)$ individual first order equations. It is preferable in numerical calculations due to its lower order. Besides, the direction characteristics and the other information is perfectly retained because all the details are displayed. The disadvantages are that all the information is mixed together and that it is more difficult for theoretical analyses than other representations.

Based on different destinations and methods, different representations of hyperbolic heat conduction can be chosen. If the theoretical analysis is to be derived, the temperature representation and the heat flux representation are better. If the vector characteristics are emphasized, the heat flux representation is a better choice. If numerical simulations are to be conducted, the hybrid representation might be a proper one. The above discussion highlights the main points which should be carefully considered when these representations are adopted.

2.3. Characteristics analyses for definition conditions

In order to get the solutions of HHCE, proper boundary conditions and initial conditions are necessary. A recognition is that the heat flux field and temperature field cannot be set at the same boundary [42]. In this paper, characteristics analyses are used to give a more detailed theoretical demonstration.

Here, in order to make it more general, an orthotropic medium is studied and 3-dimensional HHCEs are derived. It is demonstrated that the analyses for the isotropic media and the analyses for 2- or 1-dimensional heat conduction problems are only typical cases of the following method and the same conclusions are reached. The HHCEs are written as

$$\rho C_V \frac{\partial T}{\partial t} + \frac{\partial q_{x_1}}{\partial x_1} + \frac{\partial q_{x_2}}{\partial x_2} + \frac{\partial q_{x_3}}{\partial x_3} = 0, \tag{18.1}$$

$$q_{x_1} + \tau_1 \frac{\partial q_{x_1}}{\partial t} = -k_1 \frac{\partial T}{\partial x_1}, \tag{18.2}$$

$$q_{x_2} + \tau_2 \frac{\partial q_{x_2}}{\partial t} = -k_2 \frac{\partial T}{\partial x_2}, \tag{18.3}$$

$$q_{x_3} + \tau_3 \frac{\partial q_{x_3}}{\partial t} = -k_3 \frac{\partial T}{\partial x_3}. \tag{18.4}$$

It can be transformed into a form of matrix, as

$$\frac{\partial \mathbf{U}}{\partial t} + \mathbf{A}\frac{\partial \mathbf{U}}{\partial x_1} + \mathbf{B}\frac{\partial \mathbf{U}}{\partial x_2} + \mathbf{C}\frac{\partial \mathbf{U}}{\partial x_3} = \mathbf{D}, \tag{19}$$

where the matrixes are

$$\mathbf{U} = [T, q_{x_1}, q_{x_2}, q_{x_3}]^T, \tag{20.1}$$

$$\mathbf{A} = \begin{bmatrix} 0 & \frac{1}{\rho C_V} & 0 & 0 \\ \frac{k_1}{\tau_1} & 0 & 0 & 0 \\ 0 & 0 & 0 & 0 \\ 0 & 0 & 0 & 0 \end{bmatrix}, \tag{20.2}$$

$$\mathbf{B} = \begin{bmatrix} 0 & 0 & \frac{1}{\rho C_V} & 0 \\ 0 & 0 & 0 & 0 \\ \frac{k_2}{\tau_2} & 0 & 0 & 0 \\ 0 & 0 & 0 & 0 \end{bmatrix}, \tag{20.3}$$

$$\mathbf{C} = \begin{bmatrix} 0 & 0 & 0 & \frac{1}{\rho C_V} \\ 0 & 0 & 0 & 0 \\ 0 & 0 & 0 & 0 \\ \frac{k_3}{\tau_3} & 0 & 0 & 0 \end{bmatrix}, \tag{20.4}$$

$$\mathbf{D} = \begin{bmatrix} 0 & -\frac{1}{\tau_1}q_{x_1} & -\frac{1}{\tau_2}q_{x_2} & -\frac{1}{\tau_3}q_{x_3} \end{bmatrix}^T. \tag{20.5}$$

Feature faces can be found through the conversion of coordinates which transforms the variables (t, x_1, x_2, x_3) into (λ, z_1, z_2, z_3). Assume that for the feature faces the following relationships are satisfied,

$$\lambda(t, x_1, x_2, x_3) = 0, \tag{21}$$

$$\frac{\partial}{\partial t} = \frac{\partial}{\partial \lambda}\frac{\partial \lambda}{\partial t} + \frac{\partial}{\partial z_i}\frac{\partial z_i}{\partial t}, \tag{22}$$

$$\frac{\partial}{\partial x_j} = \frac{\partial}{\partial \lambda}\frac{\partial \lambda}{\partial x_j} + \frac{\partial}{\partial z_i}\frac{\partial z_i}{\partial x_j}, \tag{23}$$

where i is the dummy index and j is 1, 2 and 3, respectively. λ is the coordinate axis perpendicular to the feature faces. That is to say, the other coordinate axes are in the plane of feature faces. Eq. (21) gives a way that the information is conveyed along the face. Then Eq. (19) is transformed by Eqs. (22) and (23) into

$$\frac{\partial \mathbf{U}}{\partial \lambda}\left(\frac{\partial \lambda}{\partial t}+\mathbf{A}\frac{\partial \lambda}{\partial x_1}+\mathbf{B}\frac{\partial \lambda}{\partial x_2}+\mathbf{C}\frac{\partial \lambda}{\partial x_3}\right) + \frac{\partial \mathbf{U}}{\partial z_i}\left(\frac{\partial z_i}{\partial t}+\mathbf{A}\frac{\partial z_i}{\partial x_1}+\mathbf{B}\frac{\partial z_i}{\partial x_2}+\mathbf{C}\frac{\partial z_i}{\partial x_3}\right)=\mathbf{D}. \tag{24}$$

In the feature faces, the governing equation has nothing to do with the coordinate axes in the planes, namely perpendicular to λ. So $\frac{\partial \mathbf{U}}{\partial z_i}$ is supposed to be zero. To make sure that $\frac{\partial \mathbf{U}}{\partial \lambda}$ has more than one solution, the coefficient matrix of $\frac{\partial \mathbf{U}}{\partial \lambda}$ is supposed to have zero determinant, namely

$$\left|\mathbf{I}\frac{\partial \lambda}{\partial t}+\mathbf{A}\frac{\partial \lambda}{\partial x_1}+\mathbf{B}\frac{\partial \lambda}{\partial x_2}+\mathbf{C}\frac{\partial \lambda}{\partial x_3}\right|=0. \tag{25}$$

The vector m is set to be

$$\mathbf{m}=\left[\frac{\partial \lambda}{\partial t},\frac{\partial \lambda}{\partial x_1},\frac{\partial \lambda}{\partial x_2},\frac{\partial \lambda}{\partial x_3}\right]^{\mathrm{T}}=\left[n_t,n_{x_1},n_{x_2},n_{x_3}\right]^{\mathrm{T}}. \tag{26}$$

Then Eq. (25) are transformed into

$$|\mathbf{G}|=\begin{vmatrix} n_t & \frac{k_1}{\tau_1}n_{x_1} & \frac{k_2}{\tau_2}n_{x_2} & \frac{k_3}{\tau_3}n_{x_3} \\ \frac{n_{x_1}}{\rho C_V} & n_t & 0 & 0 \\ \frac{n_{x_2}}{\rho C_V} & 0 & n_t & 0 \\ \frac{n_{x_3}}{\rho C_V} & 0 & 0 & n_t \end{vmatrix}=0. \tag{27}$$

The roots are

$$n_{t,1}=n_{t,2}=0, \tag{28.1}$$

$$n_{t,3}=\sqrt{\frac{1}{\rho C_V}\left(\frac{k_1}{\tau_1}n_{x_1}^2+\frac{k_2}{\tau_2}n_{x_2}^2+\frac{k_3}{\tau_3}n_{x_3}^2\right)}, \tag{28.2}$$

$$n_{t,4}=-\sqrt{\frac{1}{\rho C_V}\left(\frac{k_1}{\tau_1}n_{x_1}^2+\frac{k_2}{\tau_2}n_{x_2}^2+\frac{k_3}{\tau_3}n_{x_3}^2\right)}. \tag{28.3}$$

When n_t equals zero, it means that this face is not relevant with time and in this direction, the information cannot be delivered to other places. So the boundary conditions are not necessary. When n_t is more than zero, the information is transferred from the boundary into the inner space, so a boundary condition is supposed to be proposed to give enough information. However, when n_t is less than zero, the information is transferred from the inner space to the boundary, no boundary condition is supposed to be proposed, and the variables are derived from compatibility conditions. In a three-dimensional heat conduction problem, for each side only one boundary condition is required. That is to say, at one boundary there are four independent variables, T, q_{x1}, q_{x2}, q_{x3}, but not all of them can be defined to get a well-posed problem. Accurately speaking, only one field of the four or only one kind of relationship of these four fields is supposed to be provided and if more relationships are given, they will either fail to be transmitted from the boundary or contradict the constitutive equations.

Different from fluid mechanics, the lack of convective term in CV equation determines that the interactions of heat fluxes in different directions is not sufficient, making it difficult to influence each other explicitly. So the direction parallel with the boundary is less important than the vertical direction because it is hard to deliver the information into the inner space.

The compatibility relation can also be derived by this method and the relationships between the variables in the evolution equations are established. The kernel space of G are calculated,

$$[\theta_1 \quad \theta_2 \quad \theta_3 \quad \theta_4]\mathbf{G}=0. \tag{29}$$

And the following solution vectors are obtained:
when $n_t \neq 0$,

$$\theta_1=1,\ \theta_2=-\frac{n_{x_1}}{\rho C_V n_{t,3}},\ \theta_3=-\frac{n_{x_2}}{\rho C_V n_{t,3}},\ \theta_4=-\frac{n_{x_3}}{\rho C_V n_{t,3}} \tag{30.1}$$

$$\theta_1=1,\ \theta_2=-\frac{n_{x_1}}{\rho C_V n_{t,4}},\ \theta_3=-\frac{n_{x_2}}{\rho C_V n_{t,4}},\ \theta_4=-\frac{n_{x_3}}{\rho C_V n_{t,4}} \tag{30.2}$$

when $n_t=0$,

$$\theta_1=0,\ \theta_2=1,\ \theta_3=1,\ \theta_4=-\frac{\frac{k_1}{\tau_1}n_{x_1}+\frac{k_2}{\tau_2}n_{x_2}}{\frac{k_3}{\tau_3}n_{x_3}}, \tag{30.3}$$

or

$$\theta_1=0,\ \theta_2=1,\ \theta_3=-1,\ \theta_4=-\frac{\frac{k_1}{\tau_1}n_{x_1}-\frac{k_2}{\tau_2}n_{x_2}}{\frac{k_3}{\tau_3}n_{x_3}}. \tag{30.4}$$

Compatibility relation demonstrates the relationships between these time evolution equations, and it could be derived easily by the vectors above, as

$$\boldsymbol{\alpha_1}\times\text{Eq. (18.1)}+\boldsymbol{\alpha_2}\times\text{Eq. (18.2)}+\boldsymbol{\alpha_3}\times\text{Eq. (18.3)}+\boldsymbol{\alpha_4}\times\text{Eq. (18.4)}=0. \tag{31}$$

The compatibility relation suggests how the variables change with others.

3. ADI scheme based on staggered grids

3.1. Algorithm and approach

An improved ADI scheme is here proposed specifically for hyperbolic heat conduction in this section. The hybrid representation is adopted and the whole mesh is established based on staggered grids. This scheme has three advantages. The first one is the staggered grids. Special attention are paid to the structure of calculation regime and grids for the first time, which is out of the consideration of conventional ADI method. However, it is rational in the analyses of this problem. If the energy conservation equation is integrated over the unit volume, which yields

$$\int_V\left(\rho C_v\frac{\partial T}{\partial t}\right)dV+\int_V(\nabla\cdot\vec{q})dV=0. \tag{32}$$

Gauss theorem could transform the volume integration into surface integration as

$$\frac{\partial\int_V(\rho C_v T)dV}{\partial t}+\int_S(\vec{n}\cdot\vec{q})dS=0. \tag{33}$$

From the equation above, it is found that in the control volume, the average temperature and boundary heat flux are both necessary. However, they are not defined at the same position in Eq. (33). Therefore, it is better to locate the discrete temperature field and heat flux field at staggered grids. In this paper, the temperature field is defined at the grid nodes while the heat flux field is defined between the nodes. Since the heat flux is a vector, the heat fluxes in x and y directions are denoted as q_x and q_y, placed between the nodes along x and y coordinates, respectively, as shown in Fig. 1. The advantage of this distribution is that the discrete variables are sorted into several couples, combining the heat flux constitutive equation and energy conservation equation together and making it possible to solve these equations in a simpler way. The second advantage is that the heat flux and temperature fields are expressed explicitly while in other method only the temperature field or the heat flux field is derived. As discussed above, the heat flux field cannot be derived solely from temperature field. In fact, this scheme retains the vector characteristics of heat flux. The third advantage is that the difference schemes are specially treated so that chasing method can be used instead of iteration. Although

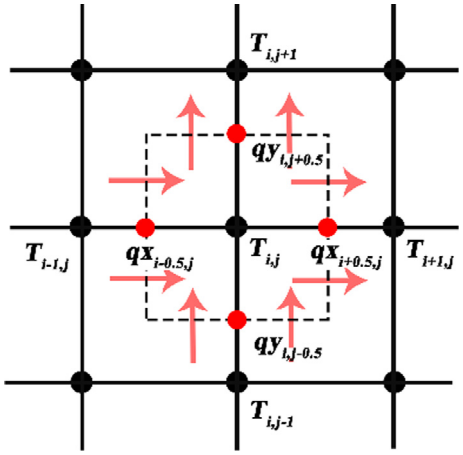

Fig. 1. The meshing sketch of discrete temperature and heat flux fields at staggered grids.

there are also disadvantages that the scheme is transformed into a conditionally stable one, it can save a lot of computing time and storage space and the convergence condition is usually satisfied after the variables are nondimensionalized.

Here the improved ADI scheme is applied to a two-dimensional transient heat conduction problem in a rectangular isotropic calculation regime. The procedure divides one temporal interval into two parts: one part from t^n to $t^{(n+1/2)}$ and the other part from $t^{(n+1/2)}$ to $t^{(n+1)}$. In the first part, T and q_x are calculated implicitly in x direction, explicitly in other directions and q_y is calculated explicitly in all directions. For convenience, the notations to be used are listed as follows:

$T^n_{i,j}$: temperature field at position (i,j) at time $t = t^n$;
$q^n_{x,i+\frac{1}{2}j}, q^n_{y,ij+\frac{1}{2}}$: heat flux field defined between the temperature nodes at time $t = t^n$;
$\delta^+_x = E^1_x - 1, \delta^-_x = 1 - E^{-1}_x$: forward difference operator and backward difference operators, where E^1_x and E^{-1}_x are shifting operators satisfying $E^1_x T^n_{i,j} = T^n_{i+1\,j}$ and $E^{-1}_x T^n_{i,j} = T^n_{i-1\,j}$;
Δt: time step;
$r_x = \frac{\Delta t}{\Delta x}, r_y = \frac{\Delta t}{\Delta y}$: step ratios in x and y directions.

The difference equation set of the hybrid representation is written as

$$\rho C_v\left(T^{n+\frac{1}{2}}_{i,j} - T^n_{i,j}\right) + \frac{1}{2} r_x \delta^-_x q^{n+\frac{1}{2}}_{x,i+\frac{1}{2}j} + \frac{1}{2} r_y \delta^-_y q^n_{y,ij+\frac{1}{2}} = 0, \tag{34.1}$$

$$\frac{1}{2}\Delta t q^n_{x,i+\frac{1}{2}j} + \tau\left(q^{n+\frac{1}{2}}_{x,i+\frac{1}{2}j} - q^n_{x,i+\frac{1}{2}j}\right) = -k r_x \delta^+_x T^{n+\frac{1}{2}}_{i,j}, \tag{34.2}$$

$$\frac{1}{2}\Delta t q^n_{y,ij+\frac{1}{2}} + \tau\left(q^{n+\frac{1}{2}}_{y,ij+\frac{1}{2}} - q^n_{y,ij+\frac{1}{2}}\right) = -k r_y \delta^+_y T^{n+\frac{1}{2}}_{i,j}. \tag{34.3}$$

Because of the staggered mesh, the locations of q_x, q_y and T are interlaced. It is found that Eqs. (34.1) and (34.2) can be solved at the same time, giving the values of q_x and T at time $t = t^{(n+1/2)}$. Then the variable q_y is solved, using the existing data of q_x and T at time $t = t^{(n+1/2)}$. Chasing method is adopted to derive the solution from Eqs. (34.1) and (34.2). The solution vector $\mathbf{z}$ is defined as the combination of temperature vector and heat flux vector in x direction,

$$\mathbf{z} = \left[q^{n+\frac{1}{2}}_{x,\frac{1}{2}j}, T^{n+\frac{1}{2}}_{1j}, q^{n+\frac{1}{2}}_{x,\frac{3}{2}j}, \ldots, q^{n+\frac{1}{2}}_{x,n-\frac{1}{2}j}, T^{n+\frac{1}{2}}_{nj}, q^{n+\frac{1}{2}}_{x,n+\frac{1}{2}j}\right] \tag{35}$$

The algebraic equation then can be rewritten into matrix form as

$$\mathbf{Bz} = \mathbf{F}, \tag{36}$$

where $\mathbf{B}$ is the coefficient matrix of solution vector $\mathbf{z}$, and $\mathbf{F}$ is the non-homogeneous term. Besides, $\mathbf{B}$ is a tridiagonal matrix, perfectly fit for chasing method. In the next step, $\mathbf{B}$ can be split into two matrixes as

$$\mathbf{B} = \mathbf{LU}, \tag{37}$$

where $\mathbf{L}$ is a lower triangular matrix and $\mathbf{U}$ is an upper triangular matrix. Both are bivariate diagonal. Eq. (36) can then be transformed into

$$\mathbf{Lw} = \mathbf{F}, \tag{38.1}$$

$$\mathbf{Uz} = \mathbf{w}, \tag{38.2}$$

where $\mathbf{w}$ is the intermediate vector variable. The algebraic equation can be solved by chasing method without iteration.

The algorithm for the part from $t = t^{(n+1/2)}$ to $t = t^{(n+1)}$ resembles the former part, where q_y and T in y direction is calculated implicitly and q_x in x direction is calculated explicitly,

$$\rho C_v\left(T^{n+1}_{i,j} - T^{n+\frac{1}{2}}_{i,j}\right) + \frac{1}{2} r_x \delta^-_x q^{n+\frac{1}{2}}_{x,i+\frac{1}{2}j} + \frac{1}{2} r_y \delta^-_y q^{n+1}_{y,ij+\frac{1}{2}} = 0, \tag{39.1}$$

$$\frac{1}{2}\Delta t q^{n+\frac{1}{2}}_{y,ij+\frac{1}{2}} + \tau\left(q^{n+1}_{y,ij+\frac{1}{2}} - q^{n+\frac{1}{2}}_{y,ij+\frac{1}{2}}\right) = -k r_y \delta^+_y T^{n+1}_{i,j}, \tag{39.2}$$

$$\frac{1}{2}\Delta t q^{n+\frac{1}{2}}_{x,i+\frac{1}{2}j} + \tau\left(q^{n+1}_{x,i+\frac{1}{2}j} - q^{n+\frac{1}{2}}_{x,i+\frac{1}{2}j}\right) = -k r_x \delta^+_x T^{n+1}_{i,j}. \tag{39.3}$$

And the chasing method is used again for the coupled Eqs. (39.1) and (39.2). The procedure for each computation time step is summarized as follows:

(1) For the part from $t = t^n$ to $t = t^{(n+1/2)}$, the partial differential equation set is discretized implicitly in x direction and explicitly in y direction.
(2) The tridiagonal system for q_x and T is solved, using the chasing method.
(3) The variable q_y is calculated from the existing data of q_x and T at time step $t = t^{(n+1/2)}$.
(4) The process (1) is repeated, but here the partial differential equation set is discretized implicitly in y direction and explicitly in x direction.
(5) The tridiagonal system for q_y and T is solved using the chasing method.
(6) The variable q_x is calculated from the existing data of q_y and T at time step $t = t^{(n+1)}$.

This method can be applied to 3-dimensional problems as well. In that case, one temporal interval are divided into three parts, namely from t^n to $t^{(n+\frac{1}{3})}$, from $t^{(n+\frac{1}{3})}$ to $t^{(n+\frac{2}{3})}$ and from $t^{(n+\frac{2}{3})}$ to $t^{(n+1)}$. The alternative direction implicit method are utilized and the following procedures are similar. The stability conditions are analyzed in the next section.

3.2. Calculation accuracy and stability condition

The calculation accuracy of the improved ADI scheme is studied. The complete difference algebraic equation set for the time from $t = t^n$ to $t = t^{(n+1)}$ is

$$\rho C_v\left(T^{n+1}_{i,j} - T^n_{i,j}\right) + r_x \delta^-_x q^{n+\frac{1}{2}}_{x,i+\frac{1}{2}j} + \frac{1}{2} r_y \delta^-_y \left(q^{n+1}_{y,ij+\frac{1}{2}} + q^n_{y,ij+\frac{1}{2}}\right) = 0, \tag{40.1}$$

$$\tau\left(q^{n+1}_{x,i+\frac{1}{2}j} - q^n_{x,i+\frac{1}{2}j}\right) = -\frac{1}{2}\Delta t\left(q^{n+\frac{1}{2}}_{x,i+\frac{1}{2}j} + q^n_{x,i+\frac{1}{2}j}\right) - k r_x \delta^+_x \left(T^{n+1}_{i,j} + T^{n+\frac{1}{2}}_{i,j}\right), \tag{40.2}$$

$$\tau\left(q^{n+1}_{y,i,j+\frac{1}{2}} - q^{n}_{y,i,j+\frac{1}{2}}\right) = -\frac{1}{2}\Delta t\left(q^{n+\frac{1}{2}}_{y,i,j+\frac{1}{2}} + q^{n+\frac{1}{2}}_{y,i,j+\frac{1}{2}}\right) - kr_y\delta_y^{+}\left(T^{n+1}_{i,j} + T^{n+\frac{1}{2}}_{i,j}\right). \tag{40.3}$$

The error term is second order in space and first order in time. Although only the forward difference and backward difference schemes are used, the spatial accuracy reaches second order due to the staggered grids. As for the stability condition, the chasing method are used to solve the tridiagonal matrix and the strongly diagonally dominant condition ensures that the chasing method is stable and valid. The following condition is supposed to be satisfied to make the coefficient matrix strongly diagonal:

$$\min(\tau/k, \rho C_V) \geqslant \max\left(\frac{\Delta t}{\Delta x}, \frac{\Delta t}{\Delta y}\right). \tag{41.1}$$

In Eq. (41.1), the media are assumed to be isotropic. When they are not, the minimum of the thermal property values in the left is required to be larger than the maximum of the grid properties in the right of the equation as shown in Eq. (41.2),

$$\min_i(\tau_i/k_i, \rho_i C_{Vi}) \geqslant \max\left(\frac{\Delta t}{\Delta x}, \frac{\Delta t}{\Delta y}\right). \tag{41.2}$$

And if this scheme is applied to 3-dimensional regimes, the stability condition becomes

$$\min(\tau/k, \rho C_V) \geqslant \frac{2}{3} \times \max\left(\frac{\Delta t}{\Delta x}, \frac{\Delta t}{\Delta y}\right), \tag{41.3}$$

which gives more flexible requirements. Before calculation, the state variables are nondimensionalized to simplify the calculations and requirements. Based on the Lax theorem, the difference equations are consistent with the partial different equations and stay stable in the calculations, so the convergence is reached.

Another advantage of this method is the boundary condition. Since at the boundary the heat flux field and the temperature field cannot be defined at the same time at one boundary because of the compatibility relation, the results obtained in Section 2.3 are satisfied automatically. There is no need to deal with the boundary condition specifically.

4. Numerical simulations and discussion

A two-dimensional rectangular regime is simulated in this section to study the vector characteristics of hyperbolic heat conduction phenomena and testify the improved ADI method. The regime is shown in Fig. 2. The variables are nondimensionalized by the following rules:

$$\begin{aligned} &x^* = x/d,\ t^* = t/t_0,\ T^* = T/T_0,\ q_x^* = q_x/q_0,\ q_y^* = q_y/q_0.\\ &k^* = k/k_0,\ \ (\rho C_v)^* = (\rho C_v)/(\rho C_v)_0,\ \ Z_q = \tau/t_0 \end{aligned} \tag{42}$$

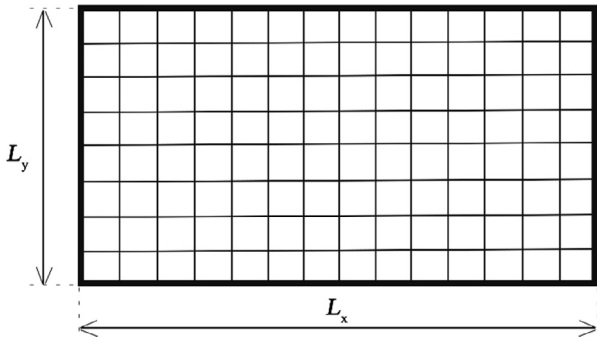

Fig. 2. The sketch of the regime and girds in two-dimensional heat conduction.

For convenience, the asterisks are uniformly omitted. The regime length L_x and L_y equals 2 and 1 respectively, with the meshing grid size reaching 0.002 × 0.002. The whole regime is set at a steady initial state with temperature T_0. All the boundaries are adiabatic if there is no specific statement.

Example 1:

The first numerical example aims to testify the improved ADI method and show the propagation phenomenon when a part of the boundary is exposed to a sine-shaped heating pulse. At the beginning, the whole regime is at an equilibrium temperature state without initial heat flux. Then a part of the left boundary, the region from 0.25 to 0.75, is heated by a laser pulse, providing a heat flux boundary condition. The heating pulse is

$$q_x = \begin{cases} A[1 - \cos(2\pi t/t_{pulse})] & t \leqslant t_{pulse} \\ 0 & t > t_{pulse} \end{cases}, \tag{43}$$

Fig. 3 shows the distribution of temperature field changing with respect to time, calculated by the ADI method. Because the thermal wave concentrates mainly in the left-half of the regime, the figures are plotted in the region [0,1] × [0,1] at time t = 0.2, 0.5 and 0.7. The value of temperature is denoted by color. It is found that the thermal wave propagates along the original direction of heat flux and maintains the shapes as time goes on. Besides, due to inhomogeneous temperature field, the heat flux in y direction appears and diffracts the thermal waves, like water ripples.

Example 2:

In this example, the disadvantage of the temperature representation is demonstrated, i.e. missing some direction information at initial state. Two initial conditions are required in temperature

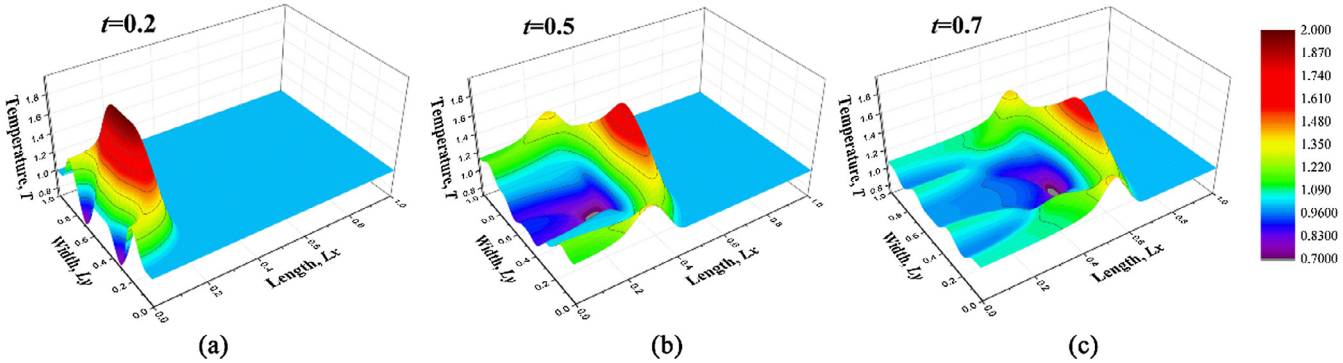

Fig. 3. The propagation profile sketches of thermal waves produced by heating half of the left boundary from y = 0.25 to y = 0.75: (a) t = 0.2, (b) t = 0.5, (c) t = 0.7.

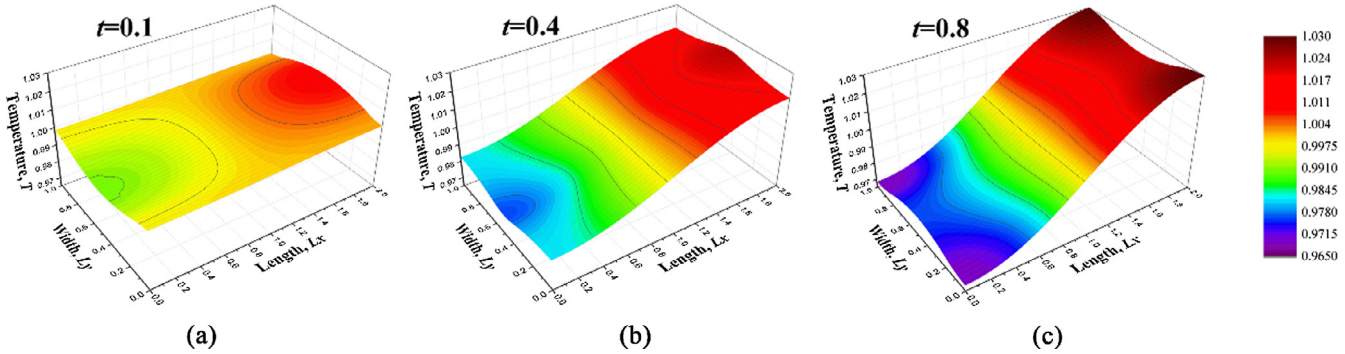

Fig. 4. The temperature field profiles of the rectangular regime under the initial condition of state 1 at different time: (a) $t = 0.1$, (b) $t = 0.4$, (c) $t = 0.8$.

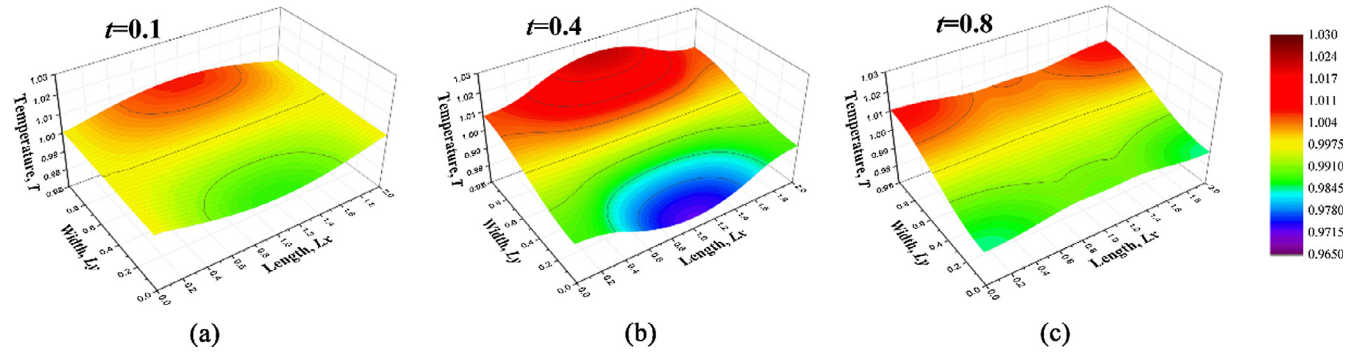

Fig. 5. The temperature field profiles of the rectangular regime under the initial condition of state 2 at different time: (a) $t = 0.1$, (b) $t = 0.4$, (c) $t = 0.8$.

representation, while the derivative of temperature field with respect to time might be confusing. According to the energy conservation equation, this derivative gives the divergence of heat flux. But it cannot depict the direction information of initial heat flux. For example, if the initial derivative of temperature with respect to time is

$$\frac{\partial T}{\partial t}(t=0,x,y) = A\sin\left(\pi\frac{x}{L_x}\right)\sin\left(\pi\frac{y}{L_y}\right), \tag{44}$$

and the initial temperature is

$$T(t=0,x,y) = T_0(x,y), \tag{45}$$

there are several couples of q_x and q_y that can produce this temperature derivative (44), among which these two are considered:

State 1:

$$q_x(t=0,x,y) = -A\frac{L_x}{\pi}\sin\left(\pi\frac{x}{L_x}\right)\sin\left(\pi\frac{y}{L_y}\right), \tag{46}$$

State 2:

$$q_y(t=0,x,y) = -A\frac{L_y}{\pi}\sin\left(\pi\frac{x}{L_x}\right)\sin\left(\pi\frac{y}{L_y}\right). \tag{47}$$

Obviously, these two states lead to different heat conduction phenomena. The simulations based on the ADI method proposed in Section 3 are conducted to give a better understanding of the difference.

The propagation sketches of temperature field profiles for different initial heat fluxes are displayed in Figs. 4 and 5 where the values of temperature field are denoted by color. Thermal waves under the initial condition of state 1 are shown in Fig. 4(a–c) while that under the initial condition of state 2 are shown in Fig. 5(a–c). Thermal waves oscillate between the adiabatic boundaries, while dissipating. Fig. 4 has the initial heat flux of q_x and the temperature field oscillates mainly along x direction. Fig. 5 has the initial heat flux of q_y and the temperature field oscillates mainly along y direction. Although the oscillation phenomena are similar, different initial heat flux directions lead to totally different energy conveying directions. Nevertheless, there is no difference between these two states if they are expressed in the temperature representation. This example reveals that the temperature representation misses the direction information of initial heat flux.

Example 3:

In this example, a new feature of hyperbolic heat conduction is considered, where the distribution of temperature gradient is not compatible with the distribution of heat flux. This situation is unphysical for Fourier's law, because the heat flux is totally determined by temperature gradient. Nevertheless, in hyperbolic heat conduction, the heat flux field is a relatively independent variable, making the incompatibility possible. By incompatibility, it means the direction of heat flux is not along the direction of temperature gradient. When a thermal wave penetrates into a medium where there already exists temperature gradients, this assumption comes true. For convenience, the calculation regime is limited to a 1×1 region. Initial heat flux and initial temperature gradient exist in the domain $(x, y) \in D[0,0.5] \times [0,0.5]$, as

$$T(t=0,x,y) = \begin{cases} (T_1 - T_0)\sin\left(2\pi\frac{x}{L_x}\right)\sin\left(2\pi\frac{y}{L_y}\right) + T_0 & (x,y) \in D \\ T_0 & (x,y) \notin D \end{cases}, \tag{48}$$

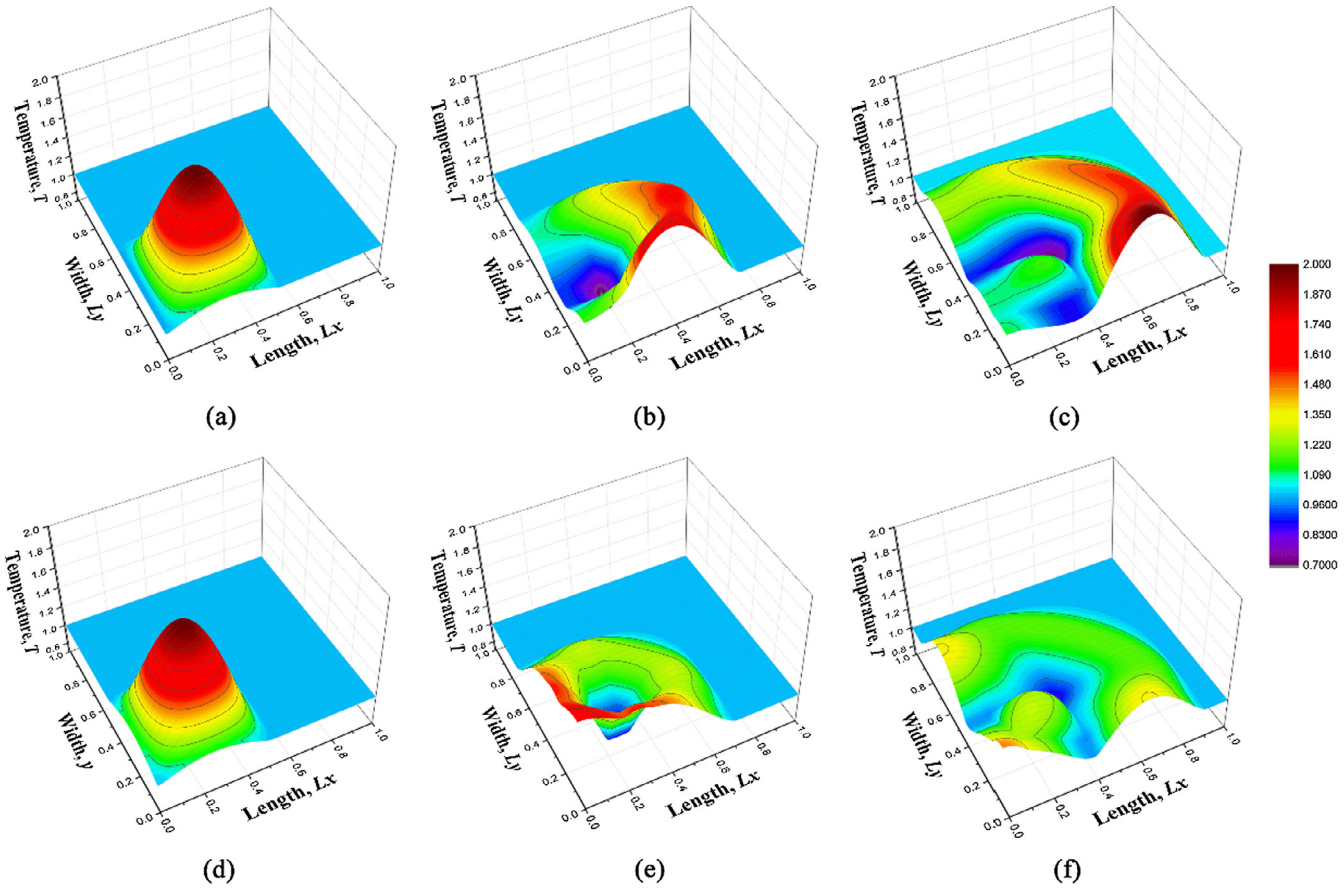

Fig. 6. The propagation sketches of temperature profile with different initial heat fluxes and temperature conditions: (a–c) with initial temperature condition and initial heat flux at time $t = 0$, 0.2 and 0.4; (d–f) with initial temperature condition and no initial heat flux at time $t = 0$, 0.2 and 0.4.

$$q_x(t=0,x,y) = \begin{cases} q_0 \sin\left(2\pi \frac{x}{L_x}\right) \sin\left(2\pi \frac{y}{L_y}\right) & (x,y) \in D \\ 0 & (x,y) \notin D \end{cases}, \tag{49.1}$$

$$q_y(t=0,x,y) = 0. \tag{49.2}$$

The control group is analyzed at the same time, where there is not initial heat flux, namely

$$q_x(t=0,x,y) = 0, \tag{50.1}$$

$$q_y(t=0,x,y) = 0. \tag{50.2}$$

The results are shown in Fig. 6. Fig. 6(a)–(c) are the temperature profiles with initial heat flux, while Fig. 6(d) and (e) are those without initial heat flux. The nondimensional time are taken as t = 0, 0.2, 0.4. The coordinate axes x and y represent the length and width of the region, and the temperature of the region is labeled by color. When there is no initial heat flux, the temperature profile propagates in a circular behavior, as shown in Fig. 6(d) and (e), while it propagates along the direction of heat flux when there exists initial heat flux, as shown in Fig. 6(a)–(c). It can be found that the propagation direction and profile pattern are altered by the appearance of initial heat flux.

When discussing the heat conduction in a plane or a body, it is important to know not only how much thermal energy is conveyed, but also where the energy goes. When there is no initial heat flux, the perturbation leaves the beginning spot and spreads like ripples without preferential direction. The thermal energy is distributed almost evenly in all possible directions. Nevertheless, initial heat flux takes effect to change the way that energy is conveyed. When the existing heat flux is not compatible with temperature gradient as shown in Fig. 6(a)–(c), the direction preference of thermal waves is obvious. The majority of thermal energy travels along the direction of heat flux, while of course some of it spreads as ripples. In this way, the energy distribution is controlled. As it is implied in the hyperbolic heat conduction equation, heat flux changes according to not only temperature gradient but also itself, which makes the phenomena different from classical Fourier heat conduction, providing new ways for heat transport manipulation.

In the above examples, the first one displays the usual propagation pattern of thermal waves in a plane when half of the boundary is exposed to a heating pulse, including dissipation and diffraction. It is found that the propagation patterns are retained for a long time due to the vector characteristics. The second one shows the advantage of the hybrid representation over the temperature representation. In this example, the initial conditions are the same in the temperature representation, while in the hybrid representation, the different directions of initial heat fluxes cause totally different propagation patterns. In the last example, the influence of initial heat flux on the way that the thermal energy is conveyed has been demonstrated. All these examples emphasize the significance of the vector characteristics of thermal waves. It was thought that the heat flux is the conjugate variable of the temperature, but in this paper, it turns out to be untrue. Heat flux field is relatively independent and sometimes mismatches with temperature field, leading to many fascinating phenomena.

Now we turn our attention to the microscopic picture of the vector characteristics of heat waves. Thermal waves propagate in the media due to the conservation of phonon momentum in dielectrics. The phonon distribution is far away from equilibrium state

and the phenomena of ballistic heat transport [2,3] and phonon hydrodynamics [58] occur. It means that phonons propagate to the boundary at the other side without collisions or through normal process. The collisions of phonons in crystal are divided into two kinds: the normal process (N process) where the phonon momentum is conserved and the resistive process (R process) where the conservation of phonon momentum is destroyed. N process dominates in phonon hydrodynamics and the main momentum is conserved. In transient heat conduction, the local temperature is defined by the local phonon energy and the local heat flux is defined by the phonon transport. If R process dominates in the media, the phonon distribution is near equilibrium Plank distribution, which is homogenous in all directions. Then the heat flux is determined by the phonon density gradient, namely the temperature gradient. Fourier's law describes this kind of heat conduction. However, if there are no collisions or N process dominates, the majority of phonon momentum is conserved and the phonon distribution cannot be described by Plank distribution because of the direction preference. The heat flux field is determined by not only the phonon density gradient, but also the historical state of phonons. The hyperbolic heat conduction equations arise and the hyperbolic behaviors imply that the thermal energy can be also transported by the original, nondissipative phonons. Therefore, the initial phonon momentum, which has a corresponding relationship with initial heat flux, is significant and the directions of phonons lead to vector characteristics. The temperature, denoting the local phonon density and the heat flux, denoting the phonon momentum both determine the thermal energy distribution patterns in hyperbolic heat conduction.

5. Conclusions

Hyperbolic heat conduction models imply that thermal energy is conveyed in wavelike behaviors. It is different from the parabolic heat conduction because of its vector characteristics, and also different from the wave propagation due to the independence of heat flux field from temperature field. In this paper, these intrinsic differences are demonstrated and the vector characteristics are highlighted. Three mathematical representations consisting of the temperature representation, the hybrid representation and the heat flux representation are analyzed, all of which are able to describe the system individually but with their own advantages and disadvantages. Characteristics analyses are adopted to give specific boundary conditions, and at the same time the feature faces and compatibility relation are found.

An improved ADI method based on staggered grids which is compatible with the physical meaning of hyperbolic heat conduction has been developed. The heat flux field and the temperature field are located at different positions, making it possible to solve these variables at the same time by chasing method. The new scheme adopts the hybrid representation and retains sufficient original transport information, perfectly demonstrating the vector characteristics. Although the stability condition of the difference scheme becomes conditional, chasing method is adopted instead of iteration, enabling to save a lot of computation time and storage memory. The scheme has second order accuracy in space and first order accuracy in time. Besides, three numerical simulations are conducted to study the influence of the vector characteristics, which imply possible ways for precise thermal energy management.

It is found that in the CV equation, the interactions among heat fluxes in different directions are rare due to the lack of convective term. In three-dimensional heat conduction problems, for each boundary only one variable or one relationship of the variables is required, and the extra boundary variable relationships might conflict with the compatibility relation. Vector characteristics are significant in hyperbolic heat conduction system, because it determines the propagation direction of the thermal energy. Vector characteristics have two significant influences. One is that during propagation, the general patterns and directions of thermal waves are retained. The other suggests that the direction in which the thermal energy is transported relies on not only the temperature gradient profile but also the heat flux direction. Due to the possible mismatch between the heat flux and the temperature gradient profiles, the propagation phenomena might be totally different even under the same initial condition expressions described by the temperature and the derivative of temperature with respect to time. It shows the influence of heat flux direction. The initial heat flux gives an obvious direction preference of energy conveying, instead of ripple-like spreading behaviors. As for the microscopic image, hyperbolic heat conduction arises due to the conservation of phonon momentum. The heat flux is determined by not only the phonon density gradient, but also the historical state of phonons and the thermal energy can be conveyed through phonon momentum conservation process. Therefore, the initial heat flux is significant because it provides the original phonon momentum and the propagation directions of phonons lead to the vector characteristics.

Conflict of interest

The authors declare that they have no conflict of interest.

Acknowledgement

This work was financially supported by the National Natural Science Foundation of China (Grant Nos. 51825601, 51676108), and the Science Fund for Creative Research Group of China (Grant No. 51621062).

References

[1] D.D. Joseph, L. Preziosi, Heat waves, Rev. Mod. Phys. 61 (1989) 41–73.
[2] D.S. Tang, Y.C. Hua, B.D. Nie, B.-Y. Cao, Phonon wave propagation in ballistic-diffusive regime, J. Appl. Phys. 119 (2016) 124301.
[3] D.S. Tang, Y.C. Hua, B.Y. Cao, Thermal wave propagation through nanofilms in ballistic-diffusive regime by Monte Carlo simulations, Int. J. Therm. Sci. 109 (2016) 81–89.
[4] D.S. Tang, B.Y. Cao, Ballistic thermal wave propagation along nanowires modeled using phonon Monte Carlo simulations, Appl. Therm. Eng. 117 (2017) 609–616.
[5] C.C. Ackerman, B. Bertman, H.A. Fairbank, R.A. Guyer, Second sound in solid helium, Phys. Rev. Lett. 16 (1966) 789–791.
[6] V. Narayanamurti, R. Dynes, Observation of second sound in bismuth, Phys. Rev. Lett. 28 (1972) 1461.
[7] D.W. Pohl, V. Irniger, Observation of second sound in NaF by means of light scattering, Phys. Rev. Lett. 36 (1976) 480.
[8] M. Chester, Second sound in solids, Phys. Rev. 131 (1963) 2013.
[9] R. Kovács, P. Ván, Second sound and ballistic heat conduction: NaF experiments revisited, Int. J. Heat Mass Transf. 117 (2018) 682–690.
[10] D.Y. Tzou, Experimental support for the lagging behavior in heat propagation, J. Thermophys. Heat Transf. 9 (1995) 686–693.
[11] J. Zhou, Y. Zhang, J.K. Chen, Non-Fourier heat conduction effect on laser-induced thermal damage in biological tissues, Numerical Heat Transf., Part A: Appl. 54 (2008) 1–19.
[12] M. Jaunich, S. Raje, K. Kim, K. Mitra, Z. Guo, Bio-heat transfer analysis during short pulse laser irradiation of tissues, Int. J. Heat Mass Transf. 51 (2008) 5511–5521.
[13] B.L. Wang, J.C. Han, A crack in a finite medium under transient non-Fourier heat conduction, Int. J. Heat Mass Transf. 55 (2012) 4631–4637.
[14] Y.K. Koh, Y. Cao, D.G. Cahill, D. Jena, Heat-transport mechanisms in superlattices, Adv. Funct. Mater. 19 (2009) 610–615.
[15] M. Ciarletta, A. Sellitto, V. Tibullo, Heat-pulse propagation in functionally graded thin layers, Int. J. Eng. Sci. 119 (2017) 78–92.
[16] C. Cattaneo, Sulla conduzione del calore, Atti Sem. Mat. Fis. Univ. Modena 3 (1948) 83–101.
[17] P. Vernotte, Paradoxes in the continuous theory of the heat equation, C.R. Acad. Sci. 246 (1958) 154–1153.
[18] R.A. Guyer, J.A. Krumhansl, Solution of the linearized phonon Boltzmann equation, Phys. Rev. 148 (1966) 766–778.

[19] R.A. Guyer, J.A. Krumhansl, Thermal conductivity, second sound, and phonon hydrodynamic phenomena in nonmetallic crystals, Phys. Rev. 148 (1966) 778–788.
[20] A. Green, N. Laws, On the entropy production inequality, Arch. Ration. Mech. Anal. 45 (1972) 47–53.
[21] D.Y. Tzou, The generalized lagging response in small-scale and high-rate heating, Int. J. Heat Mass Transf. 38 (1995) 3231–3240.
[22] S.A. Rukolaine, Unphysical effects of the dual-phase-lag model of heat conduction, Int. J. Heat Mass Transf. 78 (2014) 58–63.
[23] S.A. Rukolaine, Unphysical effects of the dual-phase-lag model of heat conduction: higher-order approximations, Int. J. Therm. Sci. 113 (2017) 83–88.
[24] R. Kovács, P. Ván, Thermodynamical consistency of the dual-phase-lag heat conduction equation, Continuum Mech. Thermodyn. (2017) 1–8.
[25] M. Fabrizio, B. Lazzari, V. Tibullo, Stability and thermodynamic restrictions for a dual-phase-lag thermal model, J. Non-Equilib. Thermodyn. 42 (2017) 243–252.
[26] B.Y. Cao, Z.Y. Guo, Equation of motion of a phonon gas and non-Fourier heat conduction, J. Appl. Phys. 102 (2007) 053503.
[27] Z.Y. Guo, Q.W. Hou, Thermal wave based on the thermomass model, J. Heat Transf. 132 (2010) 072403.
[28] Y. Dong, B.Y. Cao, Z.Y. Guo, Generalized heat conduction laws based on thermomass theory and phonon hydrodynamics, J. Appl. Phys. 110 (2011) 063504.
[29] Y. Guo, D. Jou, M. Wang, Understanding of flux-limited behaviors of heat transport in nonlinear regime, Phys. Lett. A 380 (2016) 452–457.
[30] B.D. Nie, B.Y. Cao, Reflection and refraction of a thermal wave at an ideal interface, Int. J. Heat Mass Transf. 116 (2018) 314–328.
[31] G.F. Carey, M. Tsai, Hyperbolic heat transfer with reflection, Numerical Heat Transf. 5 (2007) 309–327.
[32] M. Al-Nimr, M. Naji, S. Al-Wardat, Overshooting phenomenon in the hyperbolic heat conduction model, Jpn. J. Appl. Phys. 42 (2003) 5383.
[33] P. Zhang, M. Murakami, R.Z. Wang, Study of the transient thermal wave heat transfer in a channel immersed in a bath of superfluid helium, Int. J. Heat Mass Transf. 49 (2006) 1384–1394.
[34] B. Shen, P. Zhang, Notable physical anomalies manifested in non-Fourier heat conduction under the dual-phase-lag model, Int. J. Heat Mass Transf. 51 (2008) 1713–1727.
[35] K. Ramadan, M.d.A. Al-Nimr, Thermal wave reflection and transmission in a multilayer slab with imperfect contact using the dual-phase-lag model, Heat Transf. Eng. 30 (2009) 677–687.
[36] D. Jou, V.A. Cimmelli, A. Sellitto, Nonequilibrium temperatures and second-sound propagation along nanowires and thin layers, Phys. Lett. A 373 (2009) 4386–4392.
[37] C.-C. Ji, W. Dai, Z.-Z. Sun, Numerical method for solving the time-fractional dual-phase-lagging heat conduction equation with the temperature-jump boundary condition, J. Sci. Comput. 75 (2017) 1307–1336.
[38] M.K. Zhang, B.Y. Cao, Y.C. Guo, Numerical studies on dispersion of thermal waves, Int. J. Heat Mass Transf. 67 (2013) 1072–1082.
[39] M.K. Zhang, B.Y. Cao, Y.C. Guo, Numerical studies on damping of thermal waves, Int. J. Therm. Sci. 84 (2014) 9–20.
[40] H.Q. Yang, Solution of two-dimensional hyperbolic heat conduction by high-resolution numerical methods, Numerical Heat Transf., Part A: Appl. 21 (1992) 333–349.
[41] H.T. Chen, J.Y. Lin, Numerical solution of two-dimensional nonlinear hyperbolic heat conduction problems, Numerical Heat Transf., Part B: Fundam. 25 (1994) 287–307.
[42] W. Shen, S. Han, A numerical solution of two-dimensional hyperbolic heat conduction with non-linear boundary conditions, Heat Mass Transf. 39 (2003) 499–507.
[43] W. Wu, X. Li, Application of the time discontinuous Galerkin finite element method to heat wave simulation, Int. J. Heat Mass Transf. 49 (2006) 1679–1684.
[44] A. Moosaie, G. Atefi, A.A. Fardad, Two-dimensional non-Fourier heat conduction with arbitrary initial and periodic boundary conditions, Forsch. Ingenieurwes 72 (2008) 67–76.
[45] J. Ma, Y. Sun, J. Yang, Analytical solution of non-Fourier heat conduction in a square plate subjected to a moving laser pulse, Int. J. Heat Mass Transf. 115 (2017) 606–610.
[46] C.Y. Yang, Direct and inverse solutions of the two-dimensional hyperbolic heat conduction problems, Appl. Math. Model. 33 (2009) 2907–2918.
[47] A. Rieth, R. Kovács, T. Fülöp, Implicit numerical schemes for generalized heat conduction equations, Int. J. Heat Mass Transf. 126 (2018) 1177–1182.
[48] D.W. Peaceman, J. Rachford, H. Henry, The numerical solution of parabolic and elliptic differential equations, J. Soc. Ind. Appl. Math. 3 (1955) 28–41.
[49] M. Lees, Alternating direction methods for hyperbolic differential equations, J. Soc. Ind. Appl. Math. 10 (1962) 610–616.
[50] J. Douglas, J.E. Gunn, A general formulation of alternating direction methods, Numer. Math. 6 (1964) 428–453.
[51] R.K. Mohanty, M.K. Jain, U. Arora, An unconditionally stable ADI method for the linear hyperbolic equation in three space dimensions, Int. J. Comput. Math. 79 (2002) 133–142.
[52] R.K. Mohanty, An operator splitting method for an unconditionally stable difference scheme for a linear hyperbolic equation with variable coefficients in two space dimensions, Appl. Math. Comput. 152 (2004) 799–806.
[53] M. Ciment, S.H. Leventhal, Higher order compact implicit schemes for the wave equation, Math. Comput. 29 (1975) 985–994.
[54] D. Deng, C. Zhang, Application of a fourth-order compact ADI method to solve a two-dimensional linear hyperbolic equation, Int. J. Comput. Math. 90 (2013) 273–291.
[55] H. Ding, Y. Zhang, A new fourth-order compact finite difference scheme for the two-dimensional second-order hyperbolic equation, J. Comput. Appl. Math. 230 (2009) 626–632.
[56] G. Zhang, D. Cai, Y. Du, Improved ADI scheme for linear hyperbolic equations: extension to nonlinear cases and compact ADI schemes, J. Sci. Comput. 72 (2017) 500–521.
[57] R. Kovács, Analytic solution of Guyer-Krumhansl equation for laser flash experiments, Int. J. Heat Mass Transf. 127 (2018) 631–636.
[58] S. Lee, D. Broido, K. Esfarjani, G. Chen, Hydrodynamic phonon transport in suspended graphene, Nat. Commun. 6 (2015) 6290.